AFRL-ML-WP-TP-2006-428

COMPUTATIONAL DESIGN OF UHTC MATERIALS FOR HYPERSONIC APPLICATIONS (PREPRINT)

Triplicane A. Parthasarathy, R.J. Kerans, S. Chellapilla, and A. Roy

JANUARY 2006

Approved for public release; distribution is unlimited.

STINFO COPY

MATERIALS AND MANUFACTURING DIRECTORATE
AIR FORCE RESEARCH LABORATORY
AIR FORCE MATERIEL COMMAND
WRIGHT-PATTERSON AIR FORCE BASE, OH 45433-7750

REPORT DOCUMENTATION PAGE

Form Approved
OMB No. 0704-0188

1. REPORT DATE *(DD-MM-YY)*	2. REPORT TYPE	3. DATES COVERED *(From - To)*
January 2006	Journal Article Preprint	04/01/2001 – 01/31/2006

4. TITLE AND SUBTITLE
COMPUTATIONAL DESIGN OF UHTC MATERIALS FOR HYPERSONIC APPLICATIONS (PREPRINT)

5a. CONTRACT NUMBER
FA8650-04-D-5233
FA33615-01-C-5214

5b. GRANT NUMBER

5c. PROGRAM ELEMENT NUMBER
61102F

6. AUTHOR(S)
Triplicane A. Parthasarathy (UES Inc.)
R.J. Kerans (AFRL/MLLN)
S. Chellapilla and A. Roy (AFRL/MLBC)

5d. PROJECT NUMBER
2302

5e. TASK NUMBER
00

5f. WORK UNIT NUMBER
02

7. PERFORMING ORGANIZATION NAME(S) AND ADDRESS(ES)
UES Inc.
4401 Dayton-Xenia Rd.
Dayton, OH 45432

Ceramics Branch (AFRL/MLLN)
Metals, Ceramics, & NDE Division
Structural Materials Branch (AFRL/MLBC)
Nonmetallic Materials Division
Materials and Manufacturing Directorate
Air Force Research Laboratory, Air Force Materiel Command
Wright-Patterson Air Force Base, OH 45433-7750

8. PERFORMING ORGANIZATION REPORT NUMBER

9. SPONSORING/MONITORING AGENCY NAME(S) AND ADDRESS(ES)
Materials and Manufacturing Directorate
Air Force Research Laboratory
Air Force Materiel Command
Wright-Patterson AFB, OH 45433-7750

10. SPONSORING/MONITORING AGENCY ACRONYM(S)
AFRL-ML-WP

11. SPONSORING/MONITORING AGENCY REPORT NUMBER(S)
AFRL-ML-WP-TP-2006-428

12. DISTRIBUTION/AVAILABILITY STATEMENT
Approved for public release; distribution is unlimited.

13. SUPPLEMENTARY NOTES
This work, resulting in whole or in part from Department of the Air Force contract FA8650-04-D-5233, has been submitted to the Materials, Science, and Engineering. If this work is published, Elsevier may assert copyright. The United States has for itself and others acting on its behalf an unlimited, paid-up, nonexclusive, irrevocable worldwide license to use, modify, reproduce, release, perform, display, or disclose the work by or on behalf of the Government. All other rights are reserved by the copyright owner.

PAO Case Number: AFRL/WS 06-1017, 18 Apr 2006. Paper contains color.

14. ABSTRACT
Ultra-High Temperature Ceramics (UHTC) are attractive candidates for use as leading edge components. This work explores the possibility of using computational methods to design a structure of higher strength and toughness within the constraint of 2D isotropy. The use of low-aspect ratio bone-shaped short fibers (BSSF) to improve fracture toughness and the use of composition tailoring to increase fiber strength were analyzed. Computational models show that significant improvements in fracture toughness can be realized with an aspect ratio of 15 if the fiber strengths can be raised to 1.5 GPa. The use of a single outer layer of lower thermal expansivity composition is predicted to increase strength by a factor of two, while multilayers of reasonable thickness (10 μm) result in strengthening by a factor of 3. It is predicted that these designs will offer significant leverage to increments from processing advances. An optimal design for a 2D fibrous monolith UHTC is suggested.

15. SUBJECT TERMS
Computational Design, UHTC Materials, Hypersonic Applications

16. SECURITY CLASSIFICATION OF:			17. LIMITATION OF ABSTRACT:	18. NUMBER OF PAGES	19a. NAME OF RESPONSIBLE PERSON (Monitor)
a. REPORT	b. ABSTRACT	c. THIS PAGE			Ronald J. Kerans
Unclassified	Unclassified	Unclassified	SAR	32	19b. TELEPHONE NUMBER *(Include Area Code)* N/A

Standard Form 298 (Rev. 8-98)
Prescribed by ANSI Std. Z39-18

1.0 Introduction

The next generation of aerospace vehicles is expected to fly at or above Mach numbers of 8, using scramjet engines. At such velocities, the leading edge is expected to reach temperatures that exceed the capability of carbon/carbon composites for single use.[1] Materials within a class, known as Ultra-High Temperature Ceramics (UHTC), have very high melting points of the order of 3000°C or above, and exhibit very high thermochemical stability and resistance to evaporative erosion at temperatures of 1800º to 2000ºC.[2,3] The UHTC materials are essentially carbides, nitrides or borides of early transition metals, mainly Zr, Ta, and Hf. Due to their high melting points they are more difficult to process than conventional ceramics. Thus, although these materials were first explored in the 60s, they have only recently been of engineering interest; they are likely to be enabling in certain niche applications.[4-8]

Recent work is focused on fabricating high density monoliths of good strength.[9] These materials are not available in high strength fiber form; however polycrystalline fibers of moderate strength have been realized within the co-fired ceramics approach. In this work the possible improvements in fracture toughness of UHTC has been examined using the fibrous monolith concept with a porous interfacial layer to obtain a refractory crack deflection design.[10] A modest improvement in toughness was noted; however, as is well known, the property gains of fibrous monolithic architecture are limited to one direction with poor transverse strengths. The leading edge applications require mechanical properties that are isotropic within the plane. The use of short fibers (~100 μm in radius) randomly placed within a plane and co-fired with the matrix will yield the required 2D isotropy; however this has not been attractive since the packing efficiency drops steeply with aspect ratio.[11] There will be a significant drop in properties due to the short lengths that lower the tractions across the crack face. In this work, a computational approach was undertaken to explore the possibility of designing a

structure of UHTC materials with improved strength and toughness within the constraint of 2D isotropy and the processing constraint of co-fired ceramics.

A few recent studies present novel concepts where microstructures are tailored to enhance strength or toughness. In recent work, the possibility of using bone shaped short fibers (BSSF) to impart toughening in short fiber-reinforced composites has been using metallic wires in polymer matrices. This concept, reviewed by Zhu and Beyerlein, showed that tractions across bridged cracks are significantly improved by shaping the ends of short fibers to be like dog-bone heads.[12] Their work points to the possibility of enhancing the toughness of 2D co-fired UHTC through use of short fibers that are bone-shaped.

Meanwhile, the possibility of improving the strength of glasses through surface compressive layers has been shown to be promising by Green et al.[13] In related works, Lange and coworkers have shown that ceramics designed to be in layers of alternating compositions can have significant improvements in reliability.[14-16] These studies point to the possibility of using modulus and CTE mismatch to tailor surface compositions of UHTC to enhance strength.

In this work, computational modeling was used to predict the improvements in properties of 2D co-fired UHTC using fibers that are bone-shaped for enhanced traction and compositionally tailored for enhanced strength. An illustration of the concepts for the optimization of strength and toughness of UHTC using microstructural design is shown in Figure 1. The objective of this work was to conduct a feasibility study of the concepts illustrated in Figure 1, using numerical and analytical models. For the purposes of this work, properties of HfN and $HfC_{0.67}$ were used; however parametric studies were conducted to make more general predictions.

2.0 Toughening from Bone Shaped Short Fibers (BSSF)

The effectiveness of bone-shaped short fibers (BSSF) in improving fracture toughness compared to conventional short fibers (CSF) was studied using the following approach. The contribution to traction from a fiber that is perpendicular to the crack-face was computed, and an effective volume fraction that accounts for the obliqueness was used.

The fiber stress-displacement traction from pulling a 100 micron radius BSSF out of the matrix of the same composition with a weak interface (porous), was calculated using fiber pullout models that include progressive roughness.[17,18] Since the fiber and matrix are of the same composition, there are no residual stresses to provide friction, but interfacial roughness is expected to provide mechanical interlocking and thus frictional resistance. Nominal values for the interfacial roughness amplitude and period were used for the calculations; note that these will not affect the comparison between the CSF and BSSF.

The approach used for calculating the traction law is shown in Fig.2a. The displacement, δ, resulting from an applied load, P, is comprised of 3 parts: (1) the extension,δ_f, of that part of the fiber with uniform radius, (2) the extension, $\Delta\delta_b$, from the dog-bone head, and (3) the contribution from the fiber of uniform radius under the additional load, ΔP that arises from the resistance of the dob-bone head to sliding. The second and third contributions distinguish BSSF from CSF. All of these were computed using a the progressive roughness model detailed in ref.[17,19], which applies to this problem within the limits of the shear lag approximation.

The fiber was taken to have a radius of 100 microns, with ends that are twice the size in radius. The ends were taken to transition from 100 microns to 200 microns in radius over a distance of 100 microns (45^0 taper). The fiber pullout traction is then

obtained using the model described elsewhere.[17,20] The interface was taken to be weak (attributing to a porous interlayer) and the processing stresses were neglected (the fiber and matrix are of the same composition in a fibrous monolith), but a surface roughness of amplitude 0.2 micron and period 1 micron was assumed to account for the mechanical interlocking. The case of a short fiber without bone-shaped ends was compared with a short fiber that is bone-shaped. The maximum stress for the BSSF fibers was taken to be that which resulted in the interfacial debond crack to propagate by shear up to the end of the dog bone head. The possible failure of the BSSF at the transition region of the head was neglected. The effects of aspect ratio (L/r) and friction coefficient were calculated and compared for the two cases to study the effect of using the BSSF concept.

The results of the traction laws computed as a function of aspect ratio of the fibers, is shown in Fig.2b. The traction laws for CSF, BSSF and the continuous fiber are shown compared. The location where the broken fibers deviate from the continuous fiber result is where a conventional short fiber would pullout. The additional component to the stress-displacement curve, deviating from the continuous fiber case, is the beneficial effect due to the bone-shaped fibers. Figure 3 shows results of a parametric study where the friction coefficient was varied from 0.1 to 0.3 for four different aspect ratios. It is clear that for reasonable maximum values (2.5 GPa) for fiber strength, BSSF fibers with an aspect ratio of 15 are sufficient. However there is no benefit to using BSSF over CSF for fiber strengths less than ~1.2 GPa. A minimum strength of 1.5 GPa is required to use the concept, and a strength of 2.5 GPa is preferred for full utilization of the concept.

To determine the toughness contributions from the use of BSSF, the traction laws were used to calculate the steady state toughness using the well known relation,

$$G_{IC}^{ss} = V_f \int \sigma du \qquad (3)$$

where G_{IC} is the steady state critical strain energy release rate, V_f is the volume fraction of the fibers bridging the crack, and σ, u refer to the stress-displacement traction law for the fiber pullout. Since only a fraction of the short fibers bridge the matrix cracks, an effective volume fraction which is half of the total volume fraction was used, since the fibers are taken to lie within a 2D plane by design. The random packing efficiency for cylinders in 3D as a function of aspect ratio has been analyzed by Williams and Philipse.[11] Their simulations agree reasonably well with experimental results. Their work predicts a volume fraction in 3D of 0.51 for an aspect ratio of 10 and 0.34 for an aspect ratio of 15. Fortunately, the present work shows that there is no significant benefit beyond an aspect ratio of 15. If the fibers were aligned in 2D plane, higher volume fractions can be expected. Taking the maximum possible volume fraction to be 50% in 2D, an effective volume fraction of 25% of bridging fibers was used for the calculations.

The effect of aspect ratio and interface friction coefficient on the calculated steady-state fracture toughness for an effective volume fraction of 0.25 are shown in Figures 4. It is clear that low friction coefficient and high fiber strengths favor the concept. The results suggest that the low fracture toughness (~5 $MPam^{0.5}$) of the current state-of-the-art materials stems from the low strengths of the fibrous form of the materials. Interestingly, with improvements in fiber strengths to 1.5 GPa, significant enhancement in fracture toughness are predicted. Using BSSF fibers, an aspect ratio of 15 will be sufficient to make full utilization of the strength and obtain fracture toughnesses of the order of 15-20 $MPam^{0.5}$, provided the friction coefficient is held to 0.1. Thus these calculations suggest that fibers of strength from 1.2 to 1.5 GPa are required, and strengths up to 2.5 GPa are desirable.

3.0 Strengthening from Surface Compression

3.1 Model

The failure strength of fibrous materials is often limited by surface flaws; thus the idea is to tailor the composition to obtain compressive residual stresses at the surface. The key issue in the concept of using residual surface compression stress as a means to enhance strength is the fact that this concept results in tensile residual stresses in the core.; this might activate internal flaws to be strength limiting. To keep these tensile stresses low, the surface layer has to be made as thin as possible. However if the surface layer is too thin compared to size of critical flaws at the surface, then the beneficial effect may be insignificant. The main objective of this study was to find the optimal thickness of the surface layer with respect to the critical flaw size at the surface.

To obtain compressive residual stresses at the surface, it is necessary to have a lower thermal expansion coefficient composition at the surface compared to the core. For this study, HfN which has a CTE of 10.8 ppm/ºC was chosen as the core material and $HfC_{0.67}$ with a CTE of 7.7 ppm/ºC was selected as the surface composition.[21]

An axisymmetric model was analyzed using numerical codes based on the analytical model of Pagano and Brown.[22] Details of the procedure used to calculate the strain energy release rates can be found in Ahn et al.[23] Briefly, strain energy release rate was calculated as follows. For a given remote stress, the change in model strain energy as the crack is extended by a small putative length was computed. The difference in energy divided by the area of the crack extension is taken as the strain energy release rate. The minimum stress to obtain the critical strain energy release rate was taken to be the critical stress for fracture. The total fiber radius was fixed at 100 microns. (typical radius of fibers in current fibrous monolith designs[24,25]) The fracture toughness was taken to be 2 $MPam^{0.5}$ (typical of many polycrystal ceramics) and the

temperature differential from processing to room temperature to be 2000°C (typical processing temperatures for UHTC). The size of the strength limiting flaw was taken to be 10 microns, which will yield a typical strength to be ~400 MPa, close to that of current UHTC materials. The modulii were taken to be 311 GPa (45 Msi) for HfN and 242 GPa (35 Msi) for $HfC_{0.67}$, based on reported temperature-dependent values.[21]

To determine the optimal coating thickness, this thickness was varied from less than the critical flaw size to well above the flaw size. The stress required to initiate propagation of the surface crack was determined for each thickness. Crack propagation criteria was based on critical strain energy release rate, calculated using the assumed fracture toughness of 2 $MPam^{0.5}$ and the modulus. In addition the tensile stresses in the core and its variation with external stress was monitored. After the critical coating thickness was determined, a parametric study was conducted to study the effects of critical flaw size, fracture toughness, and fiber radius.

3.2 Results

The critical value of the remote stress required to propagate the surface flaw was taken to be the strength of the fiber. The effect of coating thickness on this critical stress is shown in Figure 5. The plot gives the critical remote stress as a function of the coating thickness. The plot also shows the variation of the residual compressive stress within the coating, as well as the residual tensile stress within the core of the fiber. The simulation could not be conducted for the case when the coating thickness was exactly equal to the crack length, due to numerical overflow arising from singularities. However, extrapolation shows that the strength is a maximum when the coating thickness equals the flaw size. The plot further shows that the strength drops drastically as the coating thickness decreases from this optimal value, but only gradually as the thickness exceeds

this value. The optimal coating thickness yields a strength that is nearly six times the base strength of the material, provided the strength is limited only by surface flaws.

It is next necessary to determine if the positive stress in the core of the fiber is sufficiently small to allow the use of this concept. For the case of a coating thickness of 10 microns, the stress in the core when the remote stress is critical (for surface flaw propagation), is shown plotted as a function of coating thickness in Fig.6a. The stresses are clearly very high, indicating the need for considering failure from internal flaws. These calculations were done using the same axisymmetric model. The calculated strength of the fiber based on internal flaw, for varying internal flaw sizes, is plotted in Fig 6b. It is seen by comparison of Fig.6a and Fig.6b, that internal flaws must be limited to less than about 1 micron, in order to realize the full benefit of the concept. If the internal flaw remains the same in size as the surface flaw, then the critical stress for fiber failure (from internal flaw) is about 750 MPa. Thus this concept helps strengthening of fibers, but for the typical situation where internal and surface flaws are same in size, the benefit is limited to a maximum of a factor of 2 in strength increment. If processing improvements result in smaller internal flaw sizes, the strength can be increased to 2 GPa at 2 micron flaw size and up to 2.8 GPa with 1 micron flaw size.

To identify regimes where the concept might apply, a parametric study was conducted. The effect of key parameters (previously assumed) on the surface flaw strengthening effect, was studied. Figure 7 shows the results. Figure 7a shows the effect of base strength (a parameter that describes processing quality); 7b shows the effect of fracture toughness, 7c shows the effect of fiber radius. It is seen that with improved processing, and thus better base strength (smaller processing flaws), the concept can be used more effectively, since the surface coating will be smaller making the internal tensile stresses very low. From Fig.7b, it is seen the lower fracture toughness materials fare better in using this concept. This arises from the fact that for a

given base strength, lower fracture toughness results in smaller flaw size and thus smaller coating thickness (which again results in lower tensile stresses in the core) From Fig.7c, larger fiber radii are seen to be beneficial. This effect is a result of the fact that for a given flaw size and hence coating thickness, larger radius results in lower internal tensile stress.

Finally the effect of temperature on the surface compressive stress is shown in Fig.7d. This result is obvious, but it is shown here to illustrate the limitation of this concept. If the strengthening is used as hedge against failure from thermal gradients and thermal shock, then the concept may be useful. In the absence of thermal gradients, no benefit is predicted at or near processing temperature.

4.0 Strengthening from Multilayers

The single surface layer prevents surface-flaw propagation, making internal flaws determine the strength. A related concept that uses multilayers may help strengthen the fibers against internal flaws was evaluated in this work. This concept is analogous to the alternating laminate concept studied by Lange and coworkers for the cases of 2D laminates and 3D spheres.[14-16] The geometry of interest here is axisymmetric (concentric cylinders), which is illustrated in Figure 5.

It is envisioned that the outer layer will be in compression to suppress surface flaws, as discussed in section 2. The case of interest then is the failure from an internal flaw. We consider here the failure of a fiber of radius, r =100 microns with n (even) alternating layers of HfN and $HfC_{0.67}$. At the center we have a tensile region which has a radius of t (=r/n). Adjacent to this layer is an annular region that extends from a radius of t to 2t. The critical flaw is one with a diameter of 4t, that covers the central tensile region and the annular compressive region surrounding it. When this flaw enters the next annular region of tensile stress, it is expected to propagate catastrophically. It

remains to calculate the critical stress, σ_{th}, required to propagate a center flaw of diameter 4t.

The stresses in the tensile and compressive regions are obtained by balancing the thermal mismatch strain, $\Delta\alpha\Delta T$, over the two materials with modulii E_+, E_- and area A_+, A_- where the subscripts + and - refer to tension and compression regions.

$$\sigma_+ = \frac{\Delta\alpha\Delta T(A_- E_- E_+)}{A_- E_- + A_+ E_+}$$
$$\sigma_- = \frac{\Delta\alpha\Delta T(A_+ E_- E_+)}{A_- E_- + A_+ E_+} \qquad \ldots \qquad (1)$$

The areas are related to the number of layers,n, and the layer thickness, t.

$$A_+ = \pi t^2 + 2\pi\left[(2t^2 + 0.5t^2) + (4t^2 + 0.5t^2) + ... + \{(n-2)t^2 + 0.5t^2\}\right]$$
$$= 2\pi t^2[0.5 + 2.5 + 4.5 + ... + (n - 1.5)]$$
$$A_- = 2\pi\left[(t^2 + 0.5t^2) + (3t^2 + 0.5t^2) + ... + \{(n-1)t^2 + 0.5t^2\}\right]$$
$$= 2\pi t^2[1.5 + 3.5 + 5.5 + ... + (n - 0.5)] \qquad \ldots \qquad (2)$$

The critical stress intensity factor, K_{ic} is given by the superposition of stress intensity factor resulting from a remote stress of (σ_{th}-σ_-) acting on the fiber with a center crack of diameter, 2a (=4t), and the stress intensity factor resulting from a pressure (σ_++σ_-) acting on the inner tensile region which has a radius c (=t), over the same crack length. The latter is obtained from Wang and Jinqiu.[26] These lead to the following equation that relates the critical stress for failure, σ_{th}, to the material parameter, K_{IC}.

$$K_{IC} = (\sigma_{th} - \sigma_-)\left[\frac{2}{\pi}\sqrt{\pi(a)}\right] +$$
$$+ (\sigma_- + \sigma_+)\left[\frac{1}{\sqrt{\pi a}\sqrt{r^2 - a^2}}\right]\left[r^2 Sin^{-1}\left(\frac{a}{r}\right) + a\sqrt{r^2 - a^2} - (r^2 - c^2)Sin^{-1}\left(\frac{a^2 - c^2}{r^2 - c^2}\right) - \sqrt{(a^2 - c^2)(r^2 - a^2)}\right]$$

… (3)

Here K_{IC} is the fracture toughness, a is the radius of the center crack (=2t), r the fiber radius, c the radius of the inner tensile region (=t), σ_{th} is the remote threshold stress at which a crack that spans the inner tensile region and two compressive regions on either side, propagates catastrophically. Rearranging, equation 3, and substituting for a=2t and c=t, the threshold stress is given by

$$\sigma_{th} = \frac{K_{IC}}{\frac{2}{\pi}\sqrt{\pi(2t)}} + \sigma_{-} - \frac{(\sigma_{-}+\sigma_{+})}{\frac{2}{\pi}\sqrt{\pi(2t)}}\left[\left\{\frac{1}{\sqrt{\pi 2t}\sqrt{r^2-4t^2}}\right\}\left\{r^2 Sin^{-1}\left(\frac{2t}{r}\right) + 2t\sqrt{r^2-4t^2} - (r^2-t^2)Sin^{-1}\left(\frac{3t^2}{r^2-t^2}\right) - \sqrt{(3t^2)(r^2-4t^2)}\right\}\right] \quad \ldots (4)$$

The first term is the strength of a fiber with a center crack of radius equal to twice the layer thickness. The other two terms modify this strength based on the residual stresses.

For the case of HfN and $HfC_{0.67}$, with a fixed fiber radius of 100 microns, the effect of increasing number of alternating layers on the predicted strengths are shown in Figure 6. Figure 6a gives the strength as a function of layer thickness and Figure 6b shows the contribution of the second and third terms, which arise from residual stresses. It is seen that the effect from residual stresses saturates after about 10 layers, with a layer thickness of 10 microns. The predicted strengths show a significant beneficial effect resulting from this concept. Strengths of the order of 1.1 GPa are predicted for layer thickness of 10 microns, which is sufficient to suppress surface flaws, and is of reasonable size for microstructural tailoring. If processing methods will allow 5 micron thick layers, strength of ~1.4 GPa can be achieved using this concept.

5.0 DISCUSSION

This work explored a computational approach to design a structure that could obtain UHTC materials that are appropriate for use as leading edge in hypersonic applications. The lack of continuous fibers of high strength makes fibrous monolith with a weak (porous) interlayer the best structure for a combination of strength and toughness. However, to obtain 2D isotropy, the use of short fibers that are randomly distributed in-plane is desired. Meanwhile, it has been shown through experiments and models that the packing density of short fibers decreases drastically with aspect ratio. This places an additional restriction on the maximum aspect ratio that can be tolerated. To obtain the maximum fracture resistance with short fibers of low aspect ratio, bone-shaped fibers are attractive. The fracture toughness obtained through such a design relies on two factors, the effective volume fraction of the fiber and the strength of the fibers. This work assumed a maximum possible effective volume fraction of 0.25 and examined the possibility of obtaining high strength fibers using composition tailoring. Using HfN and HfC0.67 as model materials from the UHTC class of materials, the maximum possible strengthening through composition tailoring was predicted and compared with strength requirements predicted for BSSF concept of toughening.

The model calculations show that dog-bone shaped short fibers (BSSF) of low aspect ratio (=15) provide significant additional tractions that could enhance fracture toughness, but only if the fibers were stronger than ~1 GPa. If the fiber strength was increased to 1.5 GPa, a reasonable value for fracture toughness of ~15 $MPam^{0.5}$ is predicted for an aspect ratio of 15.

Using HfN and $HfC_{0.67}$ to represent UHTC materials, models were used to calculate the possible strengthening. The surface compressive layers significantly increase the stress required to propagate surface flaws, provided the flaws inside the fiber do not cause failure. If the flaws inside the fiber are taken to be the same size as surface flaws, then the benefit is predicted to be limited to a maximum of a factor of 2,

which yields a strength of 750 MPa with current state of processing quality. To make full utilization of the surface compressive stresses, internal flaws must be restricted to sizes of the order of 1 micron. A parametric study showed that larger fiber diameters, lower fracture toughness and smaller processing flaws help significantly in utilizing the concept. Use of alternating layers of HfN and $HfC_{0.67}$ show that a significant gain in strength can be obtained for layer thicknesses of 10 microns, which is within the realm of processing capabilities. Strengths of 1.1 GPa can be obtained with 10 micron thick layers. Finally, modeling also shows that to make full utilization of the bone shaped short fibers, fiber strengths of the order of 2 GPa are needed. However they start to make a difference at strengths above ~1.2 GPa. Thus processing advances that can help fabricate alternating layers of thickness less than 10 microns are shown to be desirable.

The results are summarized in Figure 10, by showing the best case properties that can be realized in these UHTC materials using these concepts. The fibers where taken to be short and bone-shaped, distributed randomly but within a 2D plane to a volume fraction of 0.5. The effective volume fraction in any given direction was taken to be 0.25. The composite strength is taken to be the fiber strength multiplied by the effective volume fraction. The fibers were taken to be of HfN and coated with $HfC_{0.67}$ of varying thickness and processed at 2200ºC. The results are shown as a function of coating thickness (which equals the critical flaw size). It is seen that strengths are increased by a factor of 2x, at the current processing limits with 10 micron flaws. The strengths can be further increased up to 500 MPa if the internal flaws are reduced to 1 micron. Similarly, toughness increments from bone-shaped fibers are possible if fiber strengths of over 1.2 GPa are available. Opportunities for significant toughening exists if the fiber strengths can be increased to 2 GPa. As mentioned earlier, the key limitation is that the benefits decrease with temperature to none at the processing temperature.

6.0 SUMMARY

UHTC materials are prime materials of choice for hypersonic leading edge and other ultrahigh temperature applications such as rocket nozzles. Their high melting points make processing difficult resulting in poor strength and toughness. Some improvements have been possible using the fibrous monolith approach. However they lack strength and fracture toughness within a 2 dimensional isotropic architecture. The possibility of improving these two properties with the constraint of 2D isotropy was explored in this work, using microstructural tailoring. Several emerging materials design concepts were combined to make predictions of best case scenario for UHTC materials. A materials design where bone shaped short fibers that are randomly oriented within a 2D plane are embedded in a matrix of the same composition separated by a weak porous interface was considered. Using surface compression residual stresses increments of a factor of 2 is predicted to be possible. Further enhancements will require processing advances. The use of bone shaped fibers can enhance toughness but only if the fiber strengths exceed 1.2 GPa. The key limitation is that the beneficial effects drop with temperature.

7.0 Acknowledgments

It is a pleasure to acknowledge several useful suggestions from Dr.W.Coblenz of DARPA. We also acknowledge several useful discussions with Dr.K.Buesking (MR&D), Dr.D.B.Marshall (RSC), and Dr.G.Jefferson (UES). This work was supported in part by DARPA and in part by USAF Contract #-F33615-01-C-5214, and # FA8650-04-D-5233.

8.0 REFERNCES

1. D.J. Thomas, “Design and Analysis of UHTC Leading Edge Attachment” *NASA/CR-2002-211505* (2002).
2. J.D. Bull, D.J. Rasky, and C.C. Karika, "Stability characterization of diboride composites under high velocity atmospheric flight conditions," *24th Intern. SAMPE Technical Conference,* T1092-1106 (1992).
3. M.M. Opeka, I.G. Talkmy, E.J. Wuchina, J.A. Zaykoski, and S.J. Causey, "Mechanical, thermal and oxidation properties of refractory hafnium and zirconium compounds," *Jl. Eur. Ceram. Soc.,* **19** 2405-2414 (1999).
4. E.V. Clougherty, R.L. Pober, and L. Kaufman, "Synthesis of oxidation resistant metal diboride composites," *Trans. Met. Soc. AIME,* **242** 1077-1082 (1968).
5. S.R. Levine, E.J. Opila, M.C. Halbig, J.D. Kiser, M. Singh, and J.A. Salem, "Evaluation of ultra-high temperature ceramics for aeropropulsion use," *Jl Eur. Ceram. Soc.,* **22** 2757-2767 (2002).
6. J.R. Fenter, "Refractory diborides as engineering materials," *SAMPE Quarterly,* **2,3** [1-15] (1971).
7. E. Opilla, S. Levine, and J. Lorincz, "Oxidation of ZrB2 and HfB2-based ultra-high temperature ceramics : Effect of Ta additions," *Jl of Mater. Sci.,* **39** [19] 5969-5977 (2004).
8. R. Savino, M.D.S. Fumo, D. paterna, and M. Serpico, "Aerothermodynamic study of UHTC-based thermal protection systems," *Aerospace Sci and Tech.,* **9** 151-160 (2005).
9. A.L. Chamberlain, W.G. Fahrenholtz, G.E. Hilmas, and D.T. Ellerby, "High-strength zirconium diborired-based ceramics," *J Amer. Ceram. Soc,* **87** [6] 1170-1172 (2004).
10. W.G. Fahrenholtz, G.E. Hilmas, A.L. Chamberlain, and J.W. Zimmermann, "Processing and characterization of ZrB2-based ultra-high temperature monolithic and fibrous monolithic ceramics," *Jl of Mater. Sci.,* **39** [19] 5951-5957 (2004).
11. S.R. Williams, and A.P. Philipse, "Random packings of spheres and spherocylinders simulated by mechanical contraction," *Phys. Rev.,* **E 67** [051301] 1-9 (2003).
12. Y.T. Zhu, and I.J. Beyerlein, "Bone-shaped short fiber composites-an overview," *Mater. Sci. Eng.,* **A326** 208-227 (2002).
13. D.J. Green, R. Tandon, and V.M. Sglavo, "Crack arrest and multiple cracking in glass through the use of designed residual stress profiles," *Science,* **283** 1295-1297 (1999).
14. M.P. Rao, A.J. Sanchez-Herencia, G.E. Beltz, R.M. McMeeking, and F.F. lange, "Laminar ceramics that exhibit a threshold strength," *Science,* **286** 102-105 (1999).
15. M.P. Rao, and F.F. Lange, "Factors affecting threshold strength in laminar ceramics containing thin compressive layers," *J Amer. Ceram. Soc,* **85** [5] 1222-1228 (2002).
16. G.E. Fair, and F.F. Lange, "Ceramic Composites with Three-Dimensional Architectures Designed to Produce a Threshold StrengthI. Processing," *J Amer. Ceram. Soc,* **88** [5] 1158-1164 (2005).
17. T.A. Parthasarathy, D.B. Marshall, and R.J. Kerans, "Analysis of the Effect of Interfacial Roughness on Fiber Debonding and Sliding in Brittle Matrix Composites," *Acta Met.,* **42** [11] 3773-3784 (1994).

18. T.A. Parthasarathy, D. Barlage, P.D. Jero, and R.J. Kerans, "Effects of Interfacial Roughness Parameters on Fiber Push-out Behavior of a Model Composite," *jl of Amer. Ceram. Soc.,* **77** [12] 3232-3236 (1994).
19. T. Parthasarathy, and R.J. Kerans, "Predicted Effects of Interfacial Roughness on the Behavior of Selected Ceramic Composites," *J. Am. Ceram. Soc.,* **80** [8] 2043-2055 (1997).
20. T.A. Parthasarathy, and R.J. Kerans, "Predicted Effects of Interfacial Roughness on the Behavior of Selected Ceramic Composties," *Jl of the Amer. Ceram. Soc.,* **80** [8] 2043-2055 (1997).
21. E. Wuchina, M. Opeka, S. Causey, K. Buesking, J. Spain, A. Cull, J. Routbort, and G. Guitierrez-Mora, "Designing for ultrahigh-temperature applications: The mechanical and thermal properties of HfB2, HfCx, HfNx and aHf(N)," *J. Mater. Sci.,* **39** [5939-49] (2004).
22. N.J. Pagano, and H.W. Brown, "The Full Cell Cracking Mode in Unidirectional Brittle Matrix Composites," *Composites*, **24** [2] 69-83 (1993).
23. B.K. Ahn, W.A. Curtin, T.A. Parthasarathy, and R.E. Dutton, "Criteria for Crack Deflection/Penetration critera for Fiber-Reinforced Ceramic Matrix Composites," *Composite Sci. & Tech.,* **58** [11] 1775-1784 (1998).
24. Y.-H. Koh, H.-W. Kim, and H.-E. Kim, "Mechanical properties of fibrous monolithic Si3N4/BN ceramics with different cell boundary thicknesses," *Journal of the European Ceramic Society*, **24** 699-703 (2004).
25. J.C. McNulty, M.R. Begley, and F.W. Zok, "In-plane fracture resistance of a crossply fibrous monolith," *J Amer. Ceram. Soc*, **84** [2] 367-375 (2001).
26. Q.-Z. Wang, and C. Jinqiu, "Two general equations for deriving SIF exprressions of some axisymmetric finite domain problems," *Engineering Fracture mechanics,* **61** 619-634 (1998).

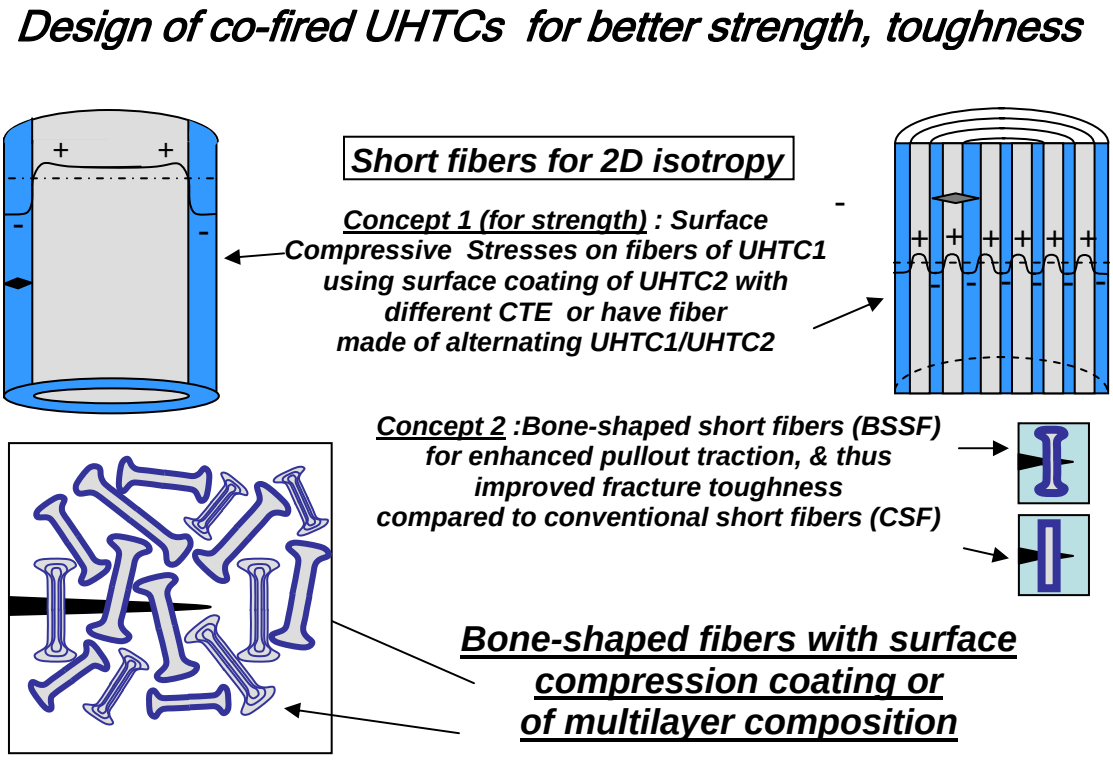

Figure 1 : The concepts of designed microstructures to realize UHTC with better strength and toughness, within the constraint of 2-dimensional isotropy required for hypersonic leading edge designs, are illustrated. The ideas of surface compression, multilayering and dog-bone shaped short fibers are combined to optimize strength and toughness

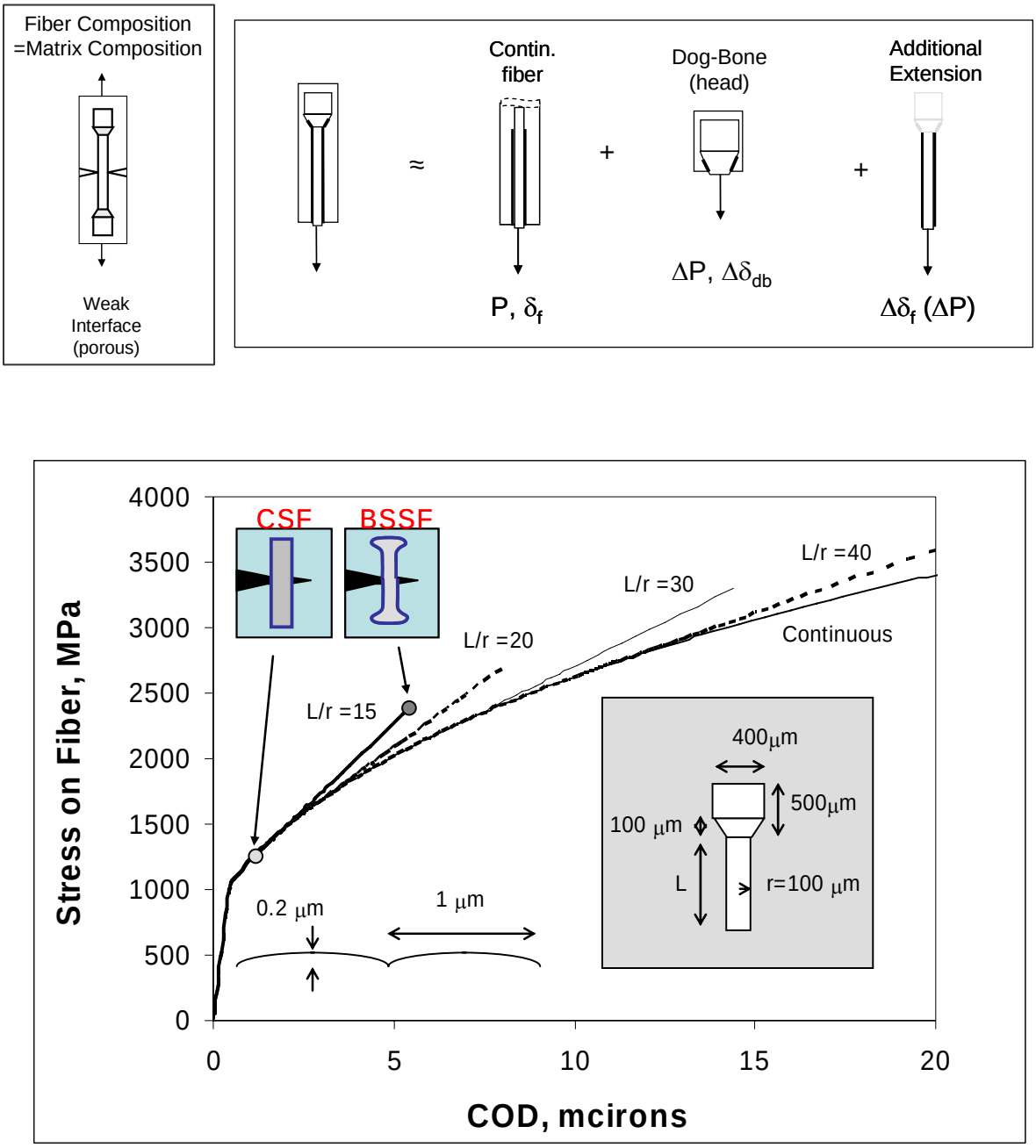

Figure 2 : The approach used to calculate the effect of bone-shaped fibers on the traction law during pullout is shown in (a). The traction law is obtained by summing the three contributions shown. (b) The calculated results are shown by comparing the traction laws for CSF, BSSF and continuous fiber. The BSSF results are also shown for different aspect ratios. It is clear that with a BSSF, an aspect ratio of 15 is sufficient, but fiber strengths of ~1.5 GPa are desirable, and ~2.5GPa are needed for full utilization of the concept.

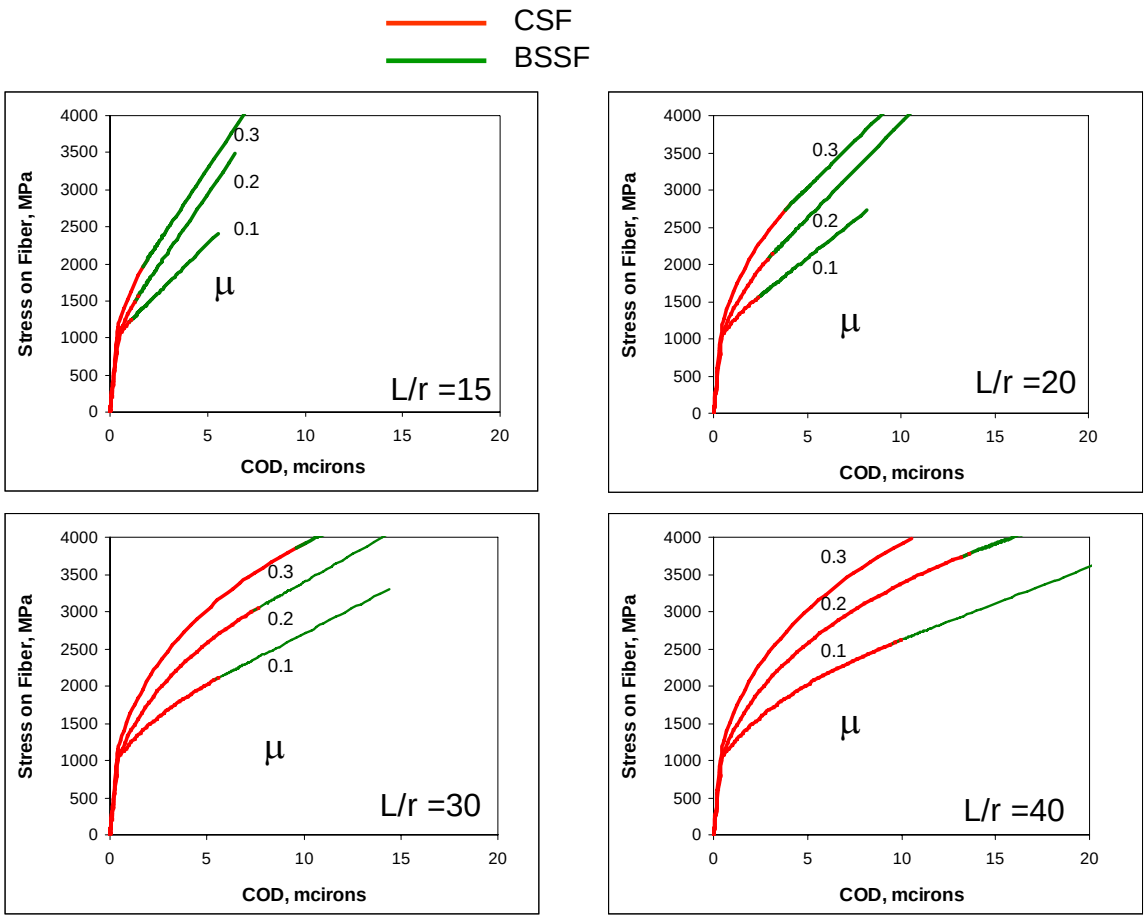

Figure 3 : The effect of friction coefficient on the stress-displacement tractions are shown for different aspect ratios of the BSSF and CSF fibers. Even for the smallest value of friction coefficient, fiber strengths of the order of 1.5 to 2.5 GPa are needed to take advantage of the BSSF concepts in UHTC materials.

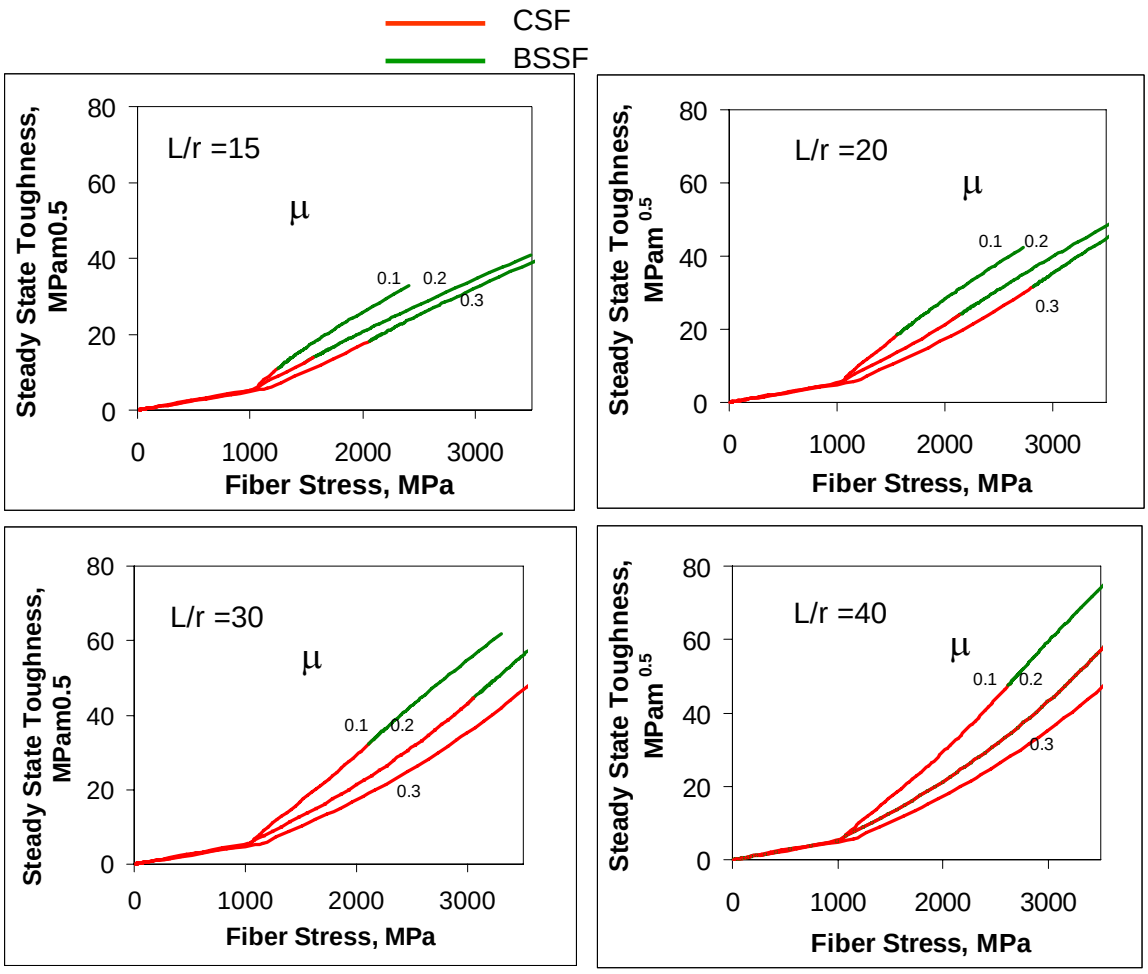

Figure 4 : The effect of friction coefficient and aspect ratio on the steady state fracture toughness ($MPam^{0.5}$) is shown as a function of maximum fiber stress. The contribution of BSSF to toughness begins only at fiber strengths above 1.2 GPa, for the low aspect ratio and low friction coefficient case. An improvement in strength to 1.5 GPa yields attractive values (>15 $MPam^{0.5}$) for fracture toughness. If strong fibers (>2 GPa) are available, the calulcations point to the possibility of significant improvement in toughness.

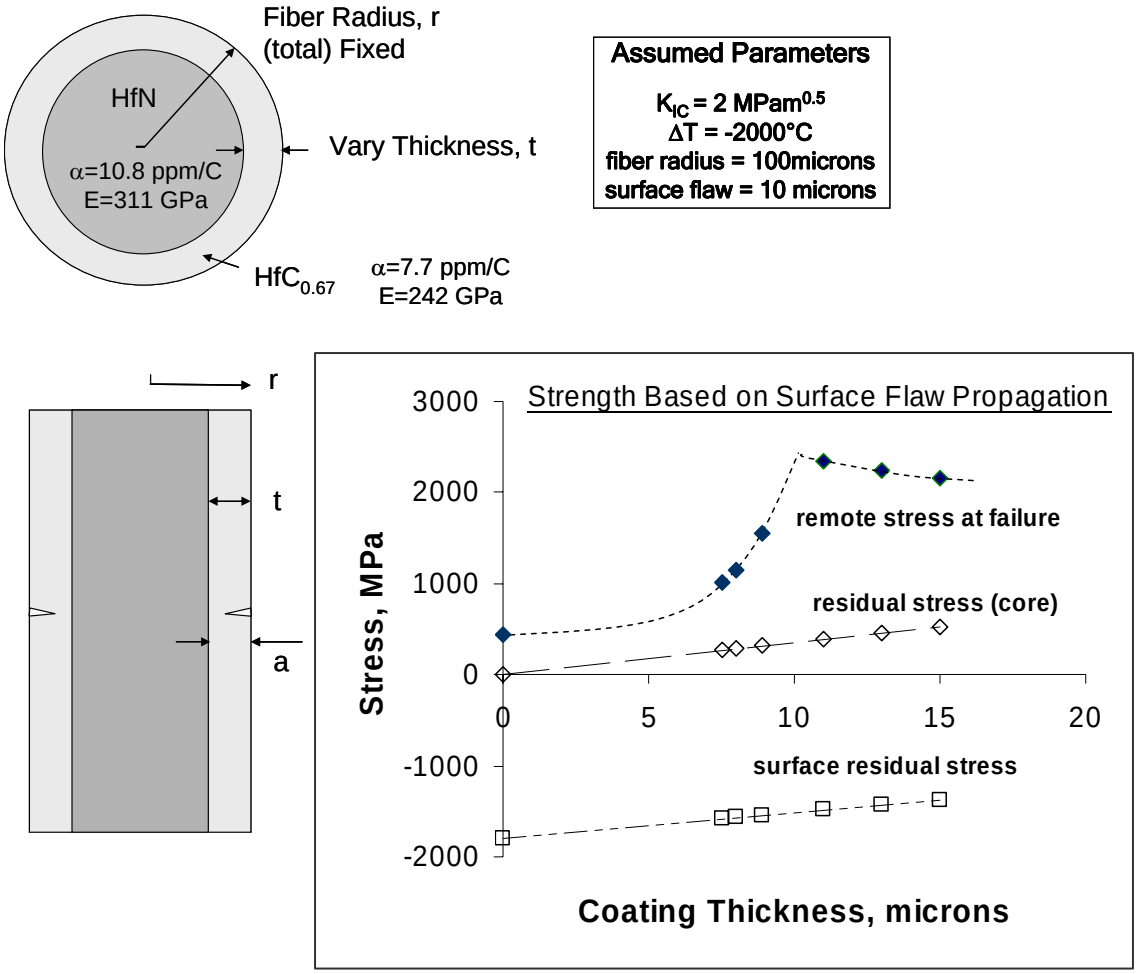

Figure 5 : The effect of coating thickness on the strength of HfN fibers coated with $HfC_{0.67}$ was calculated using the axi-symmetric damage model of Pagano and Brown.[22] The CTE mismatch results in surface compressive stress that retards surface flaw growth. The predicted strength is maximum when the coating thickness equals the surface flaw size; it is more than 5 times the uncoated strength. The residual stresses within the core and at the surface are also shown.

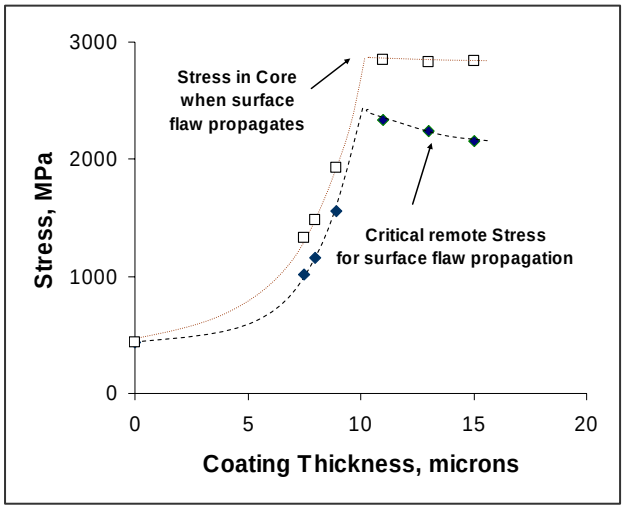

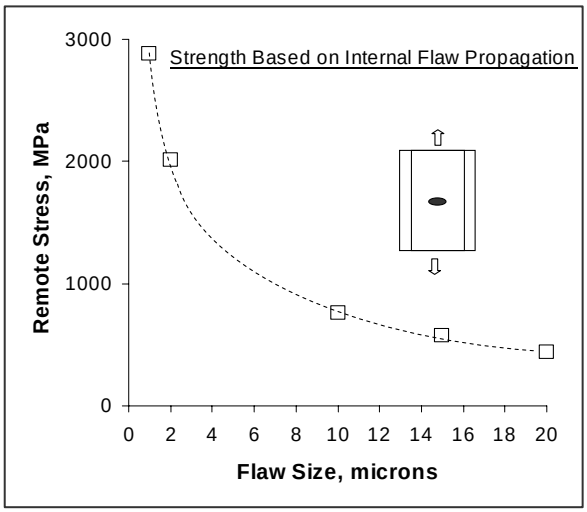

	strength (MPa)	internal flaw size (μm)	failure
No coating	436		surface
With compressive layer	759	10	internal
	2009	2	internal
	2882	1	surface

Figure 6 : The critical remote stress required to propagate flaws in a 100 micron radius HfN fiber, with a coating of $HfC_{0.67}$. (a) stress to propagate a 10 micron surface flaw, as a function of coating thickness. (b) stress required to propagate an internal flaw, as a function of flaw size, for a fixed coating thickness of 10 microns. The maximum strength of ~2.8 GPa is realized when the internal flaw is of the order of 1 micron. For a realistic scenario of internal flaw equaling surface flaw, the strength is around 750 MPa.

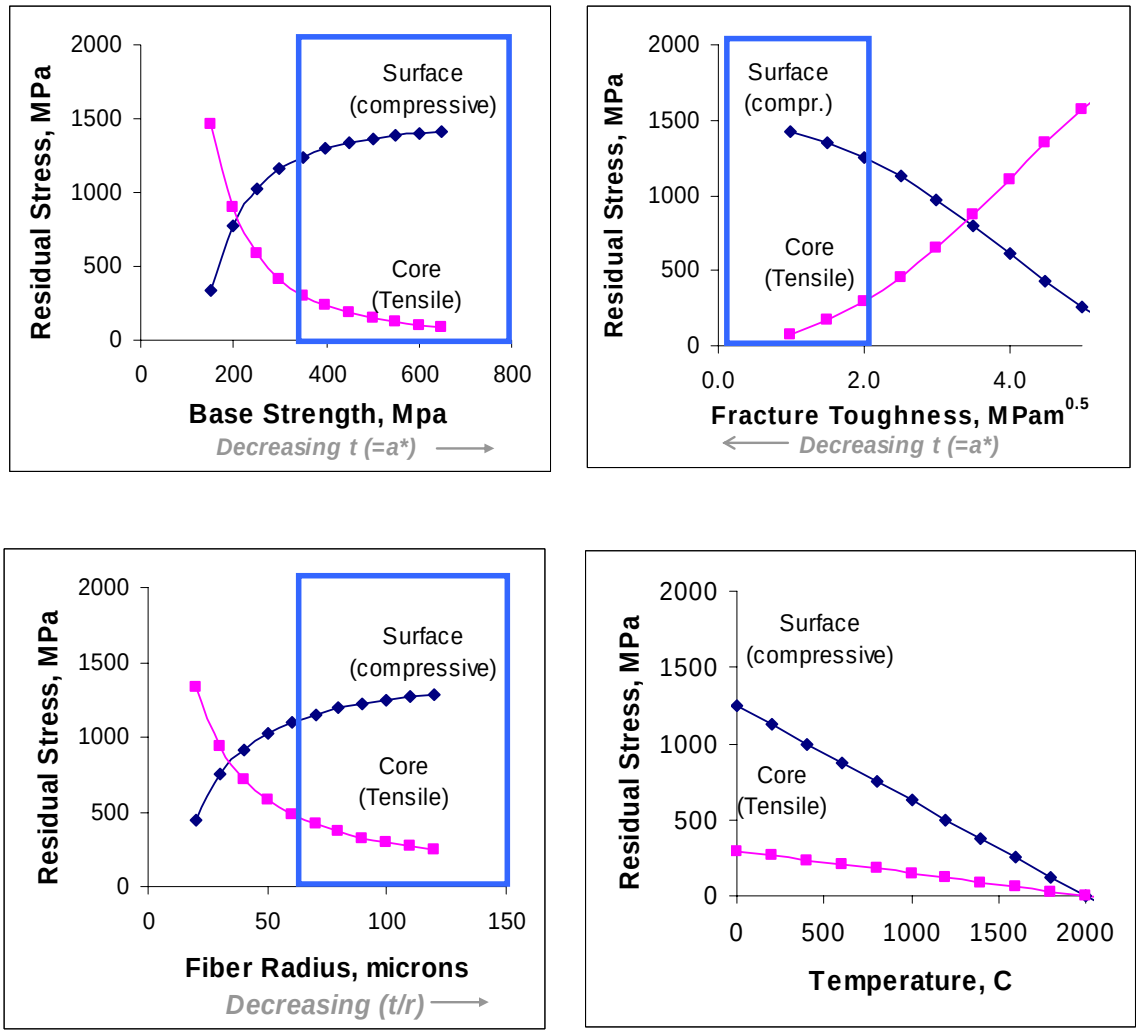

Figure 7 : The effects of (a) base strength, (b) fracture toughness, (c) fiber radius and (d) temperature on the residual stresses of a HfN fiber coated with $HfC_{0.67}$ of thickness equal to surface critical flaw size are shown. Note that the coating thickness/fiber radius varies as critical flaw size varies, which in turn depends on fracture toughness, base strength or fiber radius. In (a), (b) and (c) the effects are consistent with the fact that decreasing coating thickness (relative to fiber radius) results in higher surface compression and lower core tensile stresses. The effect of temperature is to decrease the residual stresses as the temperature nears the processing temperature. The preferred regions are shown outlined. Higher base strength, lower fracture toughness and larger fiber radii support the usefulness of the concept, while the concept offers little benefit near processing temperature.

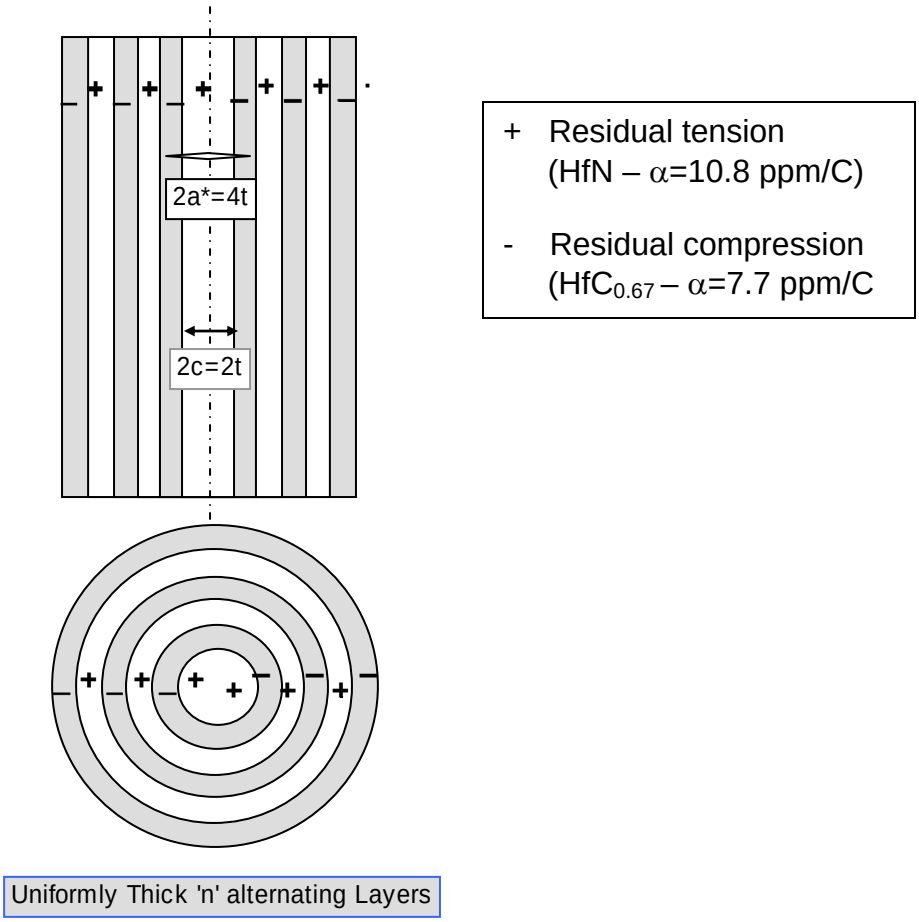

Figure 8 : The concept of multilayered architecture to strengthen UHTC fibers was examined using properties of HfN and $HfC_{0.67}$. The solution of interest is the critical stress to propagate a crack whose size is 4 times the layer thickness with the crack tip at the end of the compressive layers. The surface layers are designed to be in compression to prevent surface flaw induced failure, as detailed earlier (see Fig.2).

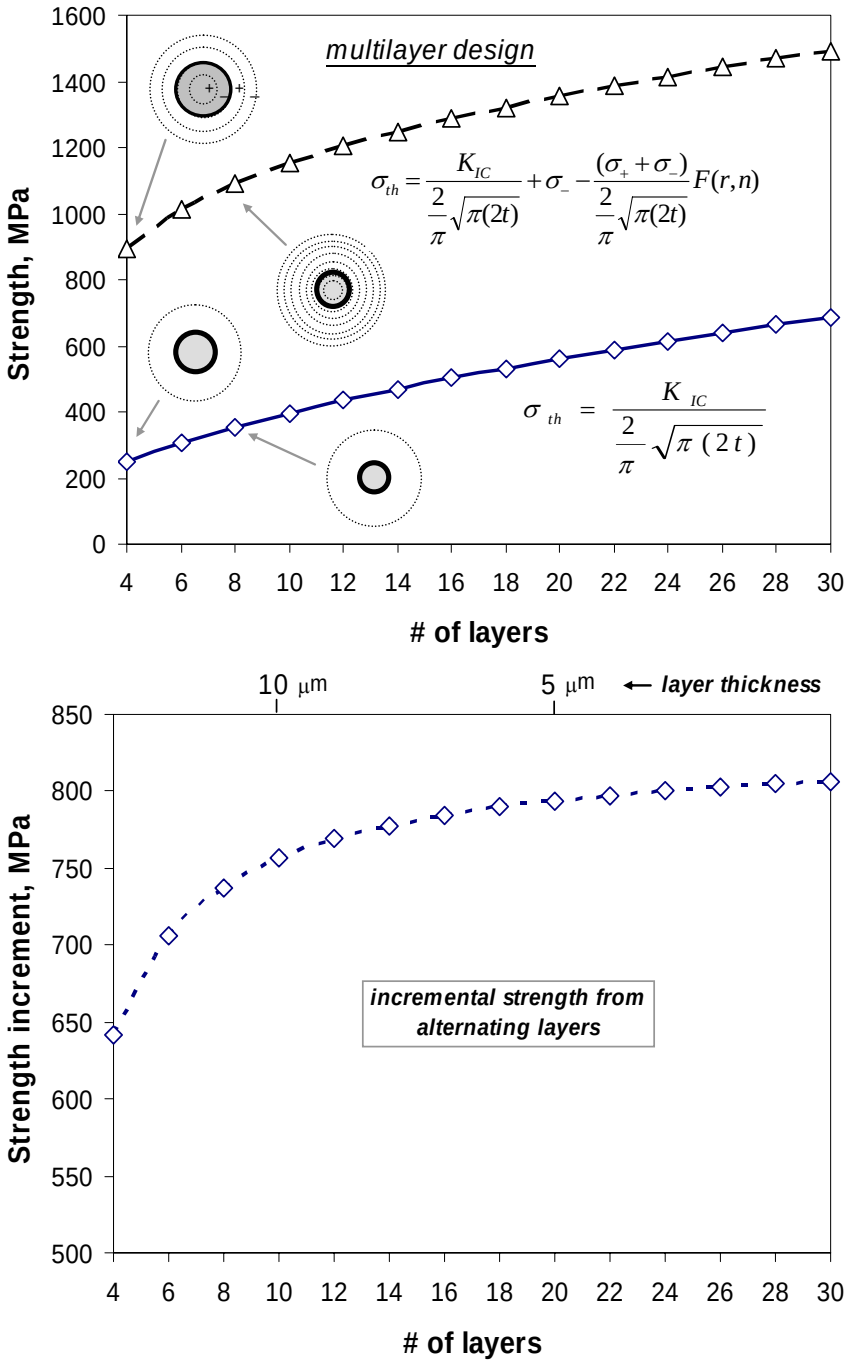

Figure 9 : (a) Predictions of the strengthening from using multilayers of HfN/$HfC_{0.67}$ are shown compared with strength without multilayers but the same flaw size. The calculations are for a fiber radius of 100 microns, with varying number (and thus thickness) of layers, and for a flaw size that is four times the layer thickness. (b) It is seen that the incremental strengthening from multilayers saturates at around 10 layers, which yields layer thickness of about 10 microns, within reach of processing. It is seen that strengths 1100 MPa are achievable using this concept, starting from for a base strength of ~300 MPa.

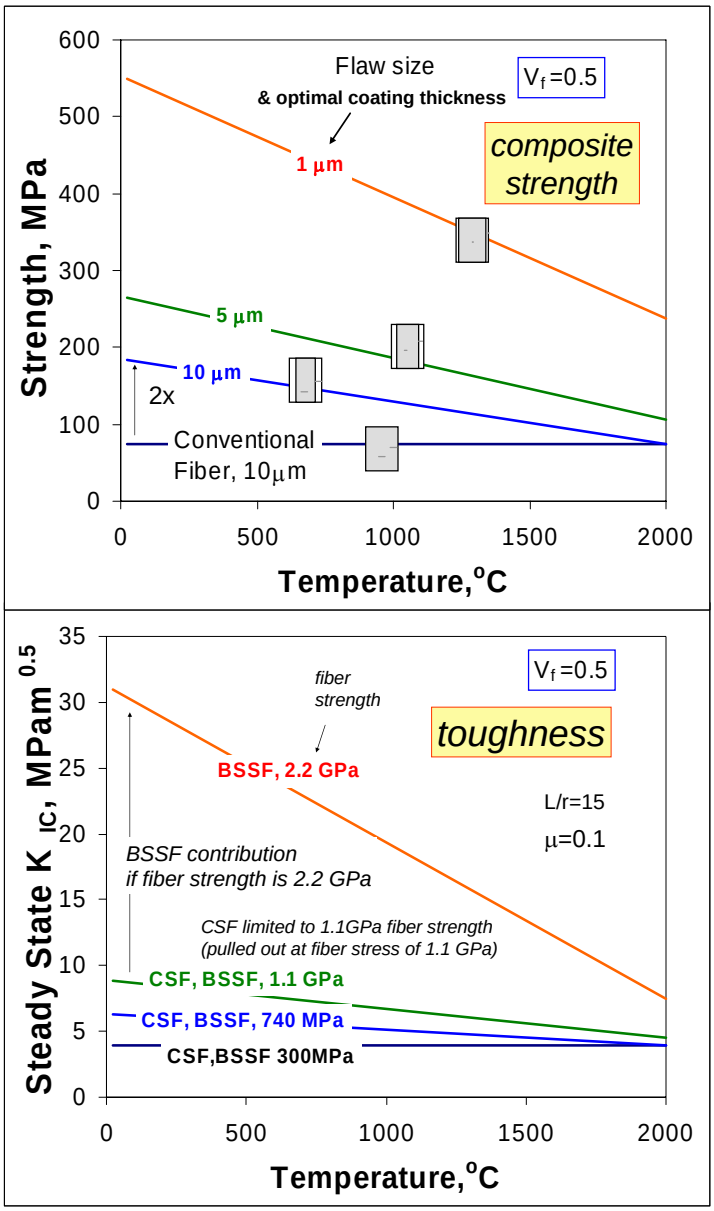

Figure 10 : A summary of the key results form this work, for a combination of HfN and $HfC_{0.67}$, are illustrated. A planar 2D isotropic design that uses a 50% fraction of random in-plane distribution of short fibers that are bone shaped and chemistry-tailored to enhance strength was considered. Using surface compressive stresses from chemical tailoring, strength improvements up to 2x are predicted, but no toughening benefit of BSSF over CSF is predicted for current processing limits. With improved processing (critical flaw sizes of the order of 1 micron), composite strengths of about 500 MPa with toughness of up to 30 $MPam^{0.5}$ are predicted.